RSC Advances

ROYAL SOCIETY OF CHEMISTRY

www.rsc.org/advances

RSC Advances

RSCPublishing

COMMUNICATION

In situ synthesis of phosphate binding mesocellular siliceous foams impregnated with iron oxide nanoparticles†

Cite this: DOI: 10.1039/x0xx00000x

Received 00th May 2014,
Accepted 00th January 2014

DOI: 10.1039/x0xx00000x

www.rsc.org/

Chee Ling Tong[a], Ela Eroglu[b,c], and Colin L. Raston[a]*

Mesocellular siliceous foams (MCFs) loaded with preformed magnetite nanoparticles ca. 8 nm in diameter are readily prepared in water under neutral conditions. The calcined composite nanomaterial with 0.72% weight of iron is effective for the adsorption of phosphate ions from liquid effluents, with the overall adsorption capacity maintained on cycling five times, up to 79.2 mg PO_4^{3-} per gram.

Mesostructured cellular foams (MCFs), also known as mesocellular foams, were developed by Stucky *et.al.* in 1998.[1] They were prepared in acidic medium, in a similar way to the synthesis of Santa Barbara Amorphous (SBA-15), under acidic condition, using 1,3,5-trimethylbenzene (TMB) as the organic co-solvent. TMB acts as a swelling agent to increase the pore size of the silica framework,[2] with the resulting MCFs having a unique three-dimensional mesostructure comprised of extensively large interconnected pore diameters of 22 to 42 nm and window diameter of 7 to 22 nm.[1-4] Subsequently in 2007, Wang *et.al.* reported success in synthesizing siliceous unilamellar vesicles and foams using a non-ionic amphiphilic copolymer as a template, in near-neutral aqueous solutions without using an organic co-solvent.[5] At the time, these mesostructured materials with significantly enlarged pore size immediately caught attention as ideal supports for catalysis, and for use in separation science and biosensors.[3-7]

Magnetic nanoparticles have a number of applications, in catalysis, biotechnology, energy and environmental remediation.[8,9] However, they tend to agglomerate due to anisotropic dipolar attractions, with loss of superparamagnetic behaviour.[10] Dispersion of such nanoparticles in a non-magnetic matrix can circumvent agglomeration, as well as protect the nanoparticles from corrosion and oxidation.[10] Impregnating magnetic nanoparticles into ordered mesoporous silica has been developed by many researchers, using a number of different methods, for example, sonochemical, temperature-programmed reduction, and grafting.[9,11] Among these, an impregnation and reduction method is successful for preparing ordered mesoporous magnetic silica nanocomposites. However, the impregnation of magnetic nanoparticles inside the pores may lead to clogging of the pores, along with decreasing the surface area and pore volume of the material.[9] Accordingly MCFs with much larger pore size have the potential to impregnate the same nanoparticles with less likelihood of clogging. Lee *et.al.* have developed a multi-step synthesis of a surface modified MFC, with γ-Fe_2O_3 nanoparticles inside the pores, which is an effective support for the immobilization of enzymes and nanoparticles.[12] Herein we have developed a robust one pot self assembly process to gain access to such MCF bearing ferromagnetic nanoparticles of hematite (Fe_2O_3) and/or its oxidized form, in targeting application in removing phosphate from waste water.

The presence of excess phosphorous in the form of phosphate ions, PO_4^{3-}, in water has the risk of initiating eutrophication.[13] Wastewater treatment using chemical precipitation for removing phosphate had its origins in Switzerland in 1950s.[9] Many other types of removal technologies have been developed since then, including physical separation, biological removal, crystallization, and ion-exchange methods.[13,14] Adsorbents for water treatment include ferric-oxides, lime, alum, zeolite, fly-ash, sand and red-mud.[8,15-19] Analogous to AsO_4^{3-},[20] PO_4^{3-} ions are effectively adsorbed on soil-minerals including the oxides of iron and aluminum.[14,16] The adsorption efficiency of the material can be enhanced by increasing its surface area, by reducing the particle size/aspect ratio,[16] and there has been increasing interest in preparing various nano-sized adsorbents. In this study, we investigate the removal of phosphate ions using MCFs incorporated with magnetic iron oxide nanoparticles. In principle, MCFs offer higher adsorption capabilities than SBA-15 due to the larger pore volume and pore diameters.[4]

The effect of adding a swelling agent such as TMB into the polymer solution during the synthesis of MCFs has been extensively studied.[2,4] We report a direct synthesis of MCFs incorporating magnetic nanoparticles *in situ* rather than as a separate process (Figure 1), with the calcined material having ultra large cavities and high pore volume which affect the physiochemical properties of the material. This is even in the absence of TMB, with a large amount of hexane used as a dispersing agent for the magnetite nanoparticles presumably acting as a pore expander in the same vein. Nevertheless, aromatic hydrocarbons are in general more solubilizing than aliphatic hydrocarbons within Pluronic micelles which features in the synthesis of MCFs.[21]

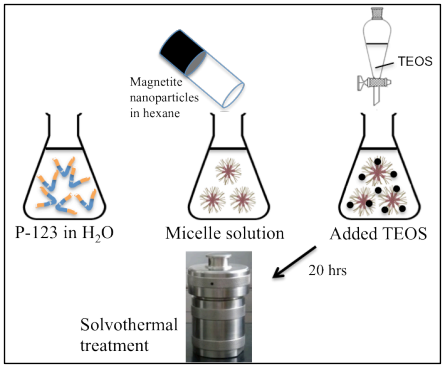

Figure 1. Schematic of the *in situ* synthesis of iron oxide loaded mesocellular siliceous foams.

Mesocellular siliceous foam loaded with magnetic nanoparticles were synthesized by modifying the procedure in the literature.[2] Firstly, 2.0 g Pluronic® P-123 ($EO_{20}PO_{70}EO_{20}$) was dissolved in 50 mL of deionized water in a 250 mL conical flask. The solution was stirred vigorously in a water bath with the temperature controlled at 40 to 45 °C to dissolve the P-123. After one hour, 10 mL of 10 mM magnetite in hexane solution (details below) was added to the P-123 solution and stirring was continued for 30 min. Thereafter, 4.4 mL of tetraethyl orthosilicate (TEOS) was added dropwise into the flask, and stirring was continued for a further 20 hours. The mixture was then transferred into a Teflon-lined autoclave and aged in an oven at 110 °C for 24 hours, with the final material being collected on cooling to room temperature via vacuum filtration. The initial synthesis of MCF in the present study had a mass ratio S1 for hexane/P123 of 3.2 and S2 for TEOS/P123 of 2.0. The resulting calcined material had a pore diameter of 28.7 nm and pore volume of 3.5 $cm^3.g^{-1}$, and is designated MCF-1. A second batch of material, designated MCF-2, involved decreasing the mass ratio of S1 and S2 to 0.8 and 1.5, respectively, which resulted in a smaller pore diameter of 13.4 nm, also with a smaller pore volume of 1.59 $cm^3.g^{-1}$. This agrees with the findings of Sridhar *et.al.*, in that as the ratio of swelling agent/P123 increases there is an increase in pore diameter, albeit using hexane in the present study rather than TMB.[4] In contrast, the pore diameter increased upon decreasing the ratio of TEOS/P123.[4] Both MCF-1 and MCF-2 exhibited type IV isotherm with H1 hysteresis loop, according to IUPAC definition, Figure 2.[22] It should be noted that the BJH method underestimates pore diameter,[23] and many reports have used the proposed modified Broekhoff-de Boer (BdB) method involving the Frenkel–Halsey–Hill (FHH) theory developed by Lukens *et.al.* for reporting the pore size distribution of mesocellular foams.[2,4,23] Nonetheless, the pore diameters in our study were calculated using the BJH method, given that there was no significant discrepancy with estimated pore diameter from transmission electron micrographs (TEM) images.

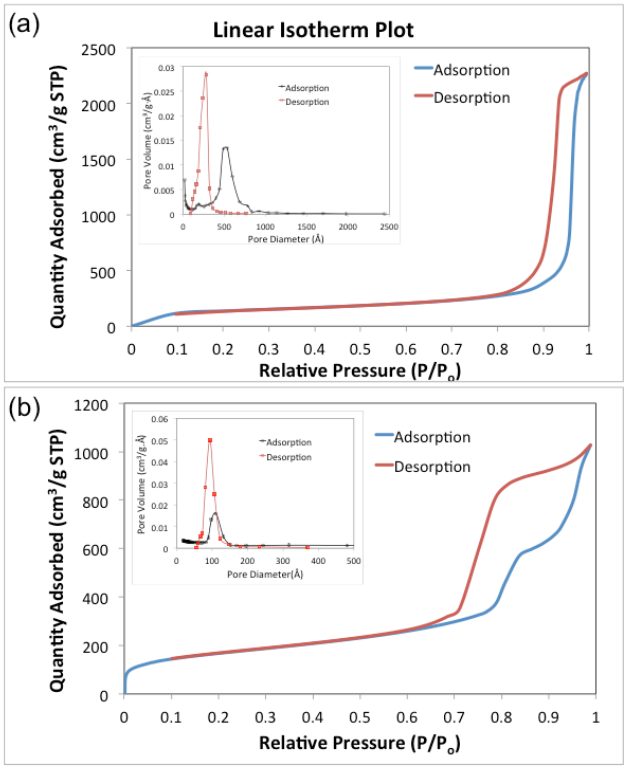

Figure 2. Nitrogen sorption isotherm for (a) MCF-1 and (b) MCF-2 showing a typical type IV hysteresis, with the corresponding pore diameter distributions of adsorption and desorption branch as an inset.

TEM of the MCFs revealed pore diameter differences resulting from using the two different ratios of hexane/P123 (Figure 3). The pores are not regularly packed, with a combination of distorted spherical cellular and indistinct polyhedral cellular foams. Structural transformation from tubules to vesicles occurred by increasing the hydrophobic volume fraction, which also depends on the temperature of the process.[5,24] When lower the concentration (ratio) of hexane, it not only results in a decrease in pore sizes, but there is now a combination of spherical pores and hexagonal packing of cylindrical pores. This relates to the presence of hexane which has high Flory-Huggins interaction parameters, being a non-ideal solvent for propylene oxide (PO) blocks in micelles.[21] This is consistent with a lower amount of hexane not dramatically enhancing (increasing) the pore diameter. Silica wall thickness determined from TEM images was around 5.0 – 5.5 nm for both samples, being independent of pore diameter.

Monodispersed magnetite was prepared using the method reported by Sun *et.al.* and re-dispersed in hexane.[25] The particle sizes determined from TEM were ca. 8 nm (ESI, Figure S1), which is consistent with the diameters determined from TEM images (inset) for the composite material, being approximately 7 – 8 nm in diameter. TEM images of the calcined MCF-1 sample showed the magnetite nanoparticles were successfully loaded within the mesocellular foam network, Figure 3. Also, a weak Fe element peak can be observed from the elemental analysis spectrum using energy-dispersive X-ray spectroscopy (EDS) under TEM (Figure S2). The amount of magnetic nanoparticles present corresponds to 0.7 wt% of the iron in final sample, as determined using ICP-MS. From SEM micrographs, MCF-1 is comprised of clusters of small spherical particles (Figure 3). Under high resolution SEM, it appears as a sponge like surface, where the spaces between the interconnected particles reflect the pore diameter of the material.

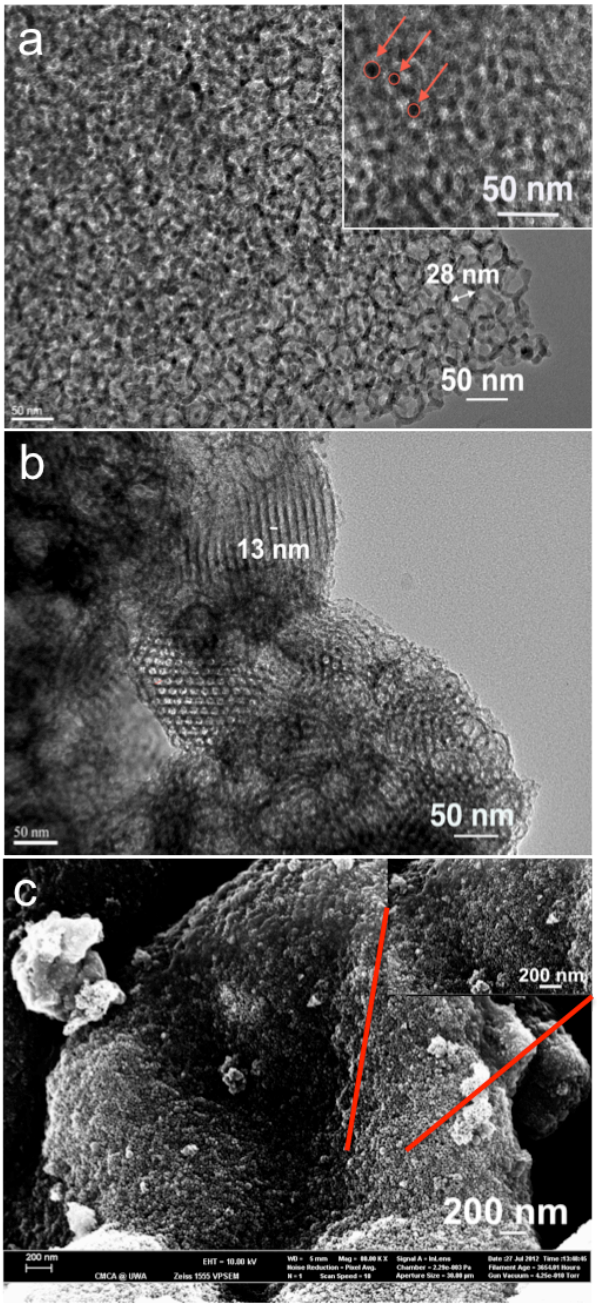

Figure 3. TEM images of (a) MCFs with S1 (see text) value at 3.2, inset showing the magnetite nanoparticles, and (b) S1 value at 0.5. (c) SEM image of MCF-1 with the magnified image of the selected area (inset).

Since the magnetite (Fe_3O_4) nanoparticles were loaded *in situ* during the synthesis of mesocellular foams and has undergone calcination at 500 ˚C under air, oxidation of magnetite to hematite (α-Fe_2O_3) will occur, although this could not be ascertained using XPS or X-ray diffraction (Figure S3), because of the low percentage of iron in the samples. However, Gallagher *et.al.* noted that heating pure magnetite above 250 ˚C in air results in the formation of thermodynamically stable α-Fe_2O_3.[26] At room temperature, MCF-1 shows a weak ferromagnetic behaviour with its saturation magnetization and coercivity being 0.22 emu/g and 13.5 Oe respectively.[27] At 5K, magnetization hysteresis loops of MCF-1 have dual characteristics of ferromagnetic behaviour with a coercivity of Hc = 150 Oe and a saturated magnetization of ~56.7 emu/g, and paramagnetic behaviour where a linear slop is observed at large applied fields (ESI, Figure S4).[27-29]

Phosphate removal experiments were conducted to evaluate the performance of the MCFs with respect to their physiochemical properties, which is provided in the supplementary information (ESI, Table S1). A blank experiment was conducted, which involved mixing the phosphate containing media with the mesoporous siliceous samples devoid of any iron oxides loading. This established that there was no significant amount of phosphate removal. Next, three different loadings of MCF-1 (10 mg; 25 mg; 50 mg) were separately mixed with phosphate containing aquatic media (1.5 mL). Data collection was based on the amount of phosphate concentration of the aqueous media at various time intervals, after being exposed to adsorbent MCF-1. Regardless of the loading concentration, MCF-1 resulted in similar phosphate removal values of around 1 mg PO_4^{3-} L^{-1} at given time-intervals (ESI, Table S2). Adsorption equilibrium was nearly reached within the first 30 minutes of the experiment. Clearly, the iron oxide nanoparticles present within the sample are the main factor responsible for the phosphate removal. Adsorption mechanisms are mainly divided into inner-sphere complexation and outer-sphere complexation.[30] The sorption of PO_4^{3-} ions on the iron oxides first takes place at the active sites on the surface, by forming complexes with surface bound OH^- ligand.[30] The fact that the phosphate adsorption did not significantly differ with various loading concentrations indicates that the iron nanoparticles were not entirely located at the active surfaces of the adsorbent, while some of them might be hindered within the internal pores of the mesocellular siliceous foams. This is supported by the observations from TEM where the iron oxides (dark contrast) were observed within the pores (Figure 3(a) and 3(b)). With such a high porosity, MCF can act as a membrane, with the PO_4^{3-} ions permeating from high concentration (outer surface) to low concentration (inner pores), involving a temperature and pressure gradient.

Since adsorption equilibrium was nearly reached within the first 30 minutes, and because it is more practical to carry out several consecutive cycles at one time, the optimal time-interval for testing the recycling potential of the adsorbent through consecutive cycles was set at 30 minutes. Used samples were then washed with deionized water which involved hand-vortexing for 1 minute, followed by removal of the supernatant after centrifugation at 9391 g for 5 minutes. The remaining samples were then mixed again with phosphate-containing aqueous media (1.5 mL), while the remaining phosphate content of the liquid sample was analysed after the first 30 minute of each cycle, Figure 4.

The increase in adsorbent loading had a positive effect on the total amount of PO_4^{3-} adsorbed. As shown in Figure 4, by the end of the fifth consecutive cycle, 50 mg of adsorbent yielded the highest overall phosphate adsorption value of 10 $mg.L^{-1}$, which was followed by 6.4 $mg.L^{-1}$ phosphate adsorption by a 25 mg sample, and 3.8 $mg.L^{-1}$ for a 10 mg sample. Since the main component responsible for the PO_4^{3-} removal is the iron oxide component, it is realistic to conclude that the adsorption capacity of the adsorbent is based on the amount of Fe present in the sample, which was 0.72% (w/w). Once phosphate-removal values were converted into adsorption capacities, a reverse correlation was observed between the adsorbent loading and the overall phosphate adsorption capacity. A 10 mg sample yielded an overall adsorption capacity of 79.2 mg PO_4^{3-} per gram Fe, followed by 53.3 mg PO_4^{3-} per gram Fe for a 25 mg sample, and 41.7 mg PO_4^{3-} per gram Fe for a 50 mg sample. These results are within the range of literature data given for adsorbents containing iron oxide nanoparticles.[8,31] In our previous

study, we found that the diatom frustules coated with magnetite nanoparticles yielded an overall adsorption capacity of around 45 mg PO_4^{3-} per gram Fe.[8] We also established that MCF-1 can continuously adsorb PO_4^{3-} ions during each consecutive cycle, while the adsorption rate was nearly doubled after the second cycle. This phenomenon aligns with the aforementioned proposed adsorption process, with the phosphate ions being initially adsorbed by the active sites of magnetic nanoparticles located on the surface of the silica, and then they diffuse into the cavities of the mesocellular foams during the recycling process, where the other magnetic nanoparticles reside. Since MCF-1 exhibits higher pore volume, it has a higher capability to continuously adsorb phosphate ions before reaching saturation. Recycling the material for consecutive mechanical-mixing and washing processes might slightly enhance the surface adsorption capacity of the adsorbent.

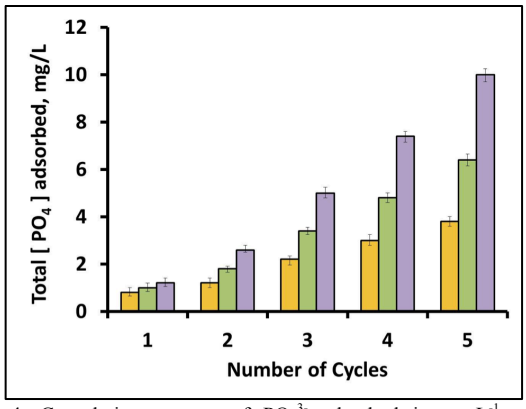

Figure 4. Cumulative amount of PO_4^{3-} adsorbed in $mg.L^{-1}$ after each consecutive cycle, for three different loading concentrations of MCF-1, for (1) 10 mg adsorbent (yellow column); (2) 25 mg adsorbent (green column); and (3) 50 mg adsorbent (purple column).

To establish whether the pore diameter would affect the overall performance, MCF-2 was synthesized with much smaller pore diameter and pore volume (ESI, Table S1). The iron content of MCF-2 determined by ICP-MS was 0.79% w/w, which was slightly higher than for MCF-1 (0.72% w/w). Given that iron oxide was the main component responsible for the phosphate removal, theoretically a slight increase in the removal rate of phosphate should be expected. The same experimental procedures were carried out, and by the end of the fifth consecutive cycle, 50 mg of MCF-2 yielded the highest overall phosphate adsorption value of 9.5 $mg.L^{-1}$, which was followed by 5.8 $mg.L^{-1}$ phosphate adsorption by a 25 mg sample, and 3.0 $mg.L^{-1}$ phosphate adsorption by a 10 mg sample, Figure 5. This establishes that MCF-2 had a slightly lower PO_4^{3-} ion adsorption capacity than MCF-1 sample, which has the larger pore sizes. Once phosphate-removal values were converted into the adsorption capacities, similar reverse correlation was observed between the adsorbent loading and the overall phosphate adsorption capacity of the adsorbent. A 10 mg sample yielded an overall adsorption capacity of 57.0 mg PO_4^{-3} per gram Fe, followed by 44.1 mg PO_4^{3-} per gram Fe for a 25 mg sample, and 36.1 mg PO_4^{3-} per gram Fe for a 50 mg sample. While the trend of the cumulative adsorption values did not show significant differences, when comparing the overall adsorption capacities per iron content, there was a significant drop in MCF-2. Presumably the smaller pore diameters hinder the adsorption and diffusion of phosphate ions towards the active sites of magnetic nanoparticles, located within the internal pores of MCF-2.

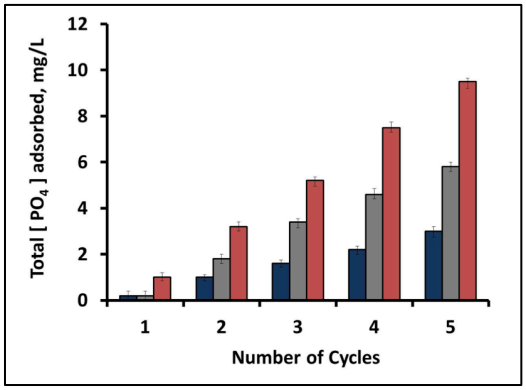

Figure 5. Cumulative amount of PO_4^{3-} adsorbed in $mg.L^{-1}$ after each consecutive cycle, for three different loading concentrations of MCF-2, (1) 10 mg adsorbent (dark-blue column); (2) 25 mg adsorbent (grey column); and (3) 50 mg adsorbent (red column).

Conclusions

In summary, we have prepared mesocellular siliceous foams under neutral conditions with *in situ* incorporation of iron oxide nanoparticles. For a minimal iron content (around 0.7% w/w), and rather small particle size (ca. 8 nm) of the magnetic nanoparticles within the siliceous foam matrix, the composite materials show a significant overall phosphate adsorption capacities of up to 79.2 mg PO_4^{3-} per gram Fe after five consecutive cycles. This process is relatively benign and cost effective, while allowing the recyclability of the adsorbent. The remaining material can be easily separated by a simple filtration step, allowing the transfer of adsorbed phosphate ions from one environment to another for further applications, including as a fertilizer.

Support from the Government of South Australia, the Australian Research Council and the Centre for Microscopy, Characterisation and Analysis (The University of Western Australia), is gratefully acknowledged, as is the preparation of the magnetite nanoparticles by Ruhani Singh.

Notes and references

[a] Flinders Centre for NanoScale Science and Technology, School of Chemical and Physical Sciences, Flinders University, Bedford Park, SA 5042, Australia. *Fax: +618-8201-2905; Tel: +618-8201-7958*;
E-mail: colin.raston@flinders.edu.au
[b] School of Chemistry and Biochemistry, The University of Western Australia, Crawley, WA 6009, Australia.
[c] ARC Centre of Excellence in Plant Energy Biology, The University of Western Australia, Crawley, WA 6009, Australia.
Electronic Supplementary Information (ESI) available: Synthesis details and characterization data. See DOI: 10.1039/c000000x/
† Dedicated to the memory of Professor Michael Lappert FRS

1. P. Schmidt-Winkel, W. W. Lukens, D. Zhao, P. Yang, B. F. Chmelka and G. D. Stucky, *J. Am. Chem. Soc.*, 1998, **121**, 254-255.
2. J. S. Lettow, Y. J. Han, P. Schmidt-Winkel, P. Yang, D. Zhao, G. D. Stucky and J. Y. Ying, *Langmuir*, 2000, **16**, 8291-8295.
3. N. Erathodiyil, S. Ooi, A. M. Seayad, Y. Han, S. S. Lee and J. Y. Ying, *Chem. Eur. J.*, 2008, **14**, 3118-3125.
4. M. Sridhar, G. K. Reddy, N. Hu, A. Motahari, D. W. Schaefer, S. W. Thiel and P. G. Smirniotis, *Microporous Mesoporous Mater.*, 2014, **190**, 215-226.
5. H. Wang, Y. Wang, X. Zhou, L. Zhou, J. Tang, J. Lei and C. Yu, *Adv. Funct. Mater.*, 2007, 17, 613-617.

6. Y. Han, S. S. Lee and J. Y. Ying, *Chem Mater.*, 2006, **18**, 643-649.
7. S. Wu, H. X. Ju and Y. Liu, *Adv. Funct. Mater.*, 2007, **17**, 585-592.
8. J. Toster, I. Kusumawardani, E. Eroglu, K. S. Iyer, F. Rosei and C. L. Raston, *Green Chem.*, 2014, **16**, 82-85.
9. J. Liu, S. Z. Qiao, Q. H. Hu and G. Q. Lu, *Small*, 2011, **7**, 425-443.
10. J. Sung Lee, S. Ki Hong, N. Jung Hur, W.-S. Seo and H. Jin Hwang, *Mater. Lett.*, 2013, **112**, 153-157.
11. I. Ursachi, A. Vasile, H. Chiriac, P. Postolache and A. Stancu, *Mater. Res. Bull.*, 2010, **46**, 2468-2473.
12. S. S. Lee, S. N. Riduan, N. Erathodiyil, J. Lim, J. L. Cheong, J. Cha, Y. Han and J. Y. Ying, *Chem. Eur. J.*, 2012, **18**, 7394-7403.
13. L. Zeng, X. Li and J. Liu, *Water Res.*, 2004, **38**, 1318-1326.
14. G. K. Morse, S. W. Brett, J. A. Guy and J. N. Lester, *Sci. Total Environ.*, 1998, **212**, 69-81.
15. S. K. Kang, K. H. Choo and K. H. Lim, *Sep. Sci. Technol.*, 2003, **38**, 3853-3874.
16. A. Zach-Maor, R. Semiat and H. Shemer, *J. Colloid Interface Sci.*, 2011, **357**, 440-446.
17. J. Xiong, Z. He, Q. Mahmood, D. Liu, X. Yang and E. Islam, *J. Hazard. Mater.*, 2008, **152**, 211-215.
18. E. W. Shin, J. S. Han, M. Jang, S.-H. Min, J. K. Park and R. M. Rowell, *Environ. Sci. Technol.*, 2003, **38**, 912-917.
19. W. Huang, S. Wang, Z. Zhu, L. Li, X. Yao, V. Rudolph and F. Haghseresht, *J. Hazard Mater.*, 2008, **158**, 35-42.
20. A. Violante and M. Pigna, Soil Sci. Soc. Am. J., 2002, **66**, 1788-1796.
21. R. Nagarajan, *Polym. Adv. Technol.*, 2001, **12**, 23-43.
22. Z. Luan, E. M. Maes, P. A. W. van der Heide, D. Zhao, R. S. Czernuszewicz and L. Kevan, *Chem. Mater.*, 1999, **11**, 3680-3686.
23. W. W. Lukens, P. Schmidt-Winkel, D. Zhao, J. Feng and G. D. Stucky, *Langmuir*, 1999, **15**, 5403-5409.
24. R. W. Corkery and A. Fogden, *Langmuir*, 2008, **24**, 10443-10452.
25. S. Sun, H. Zeng, D. B. Robinson, S. Raoux, P. M. Rice, S. X. Wang and G. Li, *J. Am. Chem. Soc.*, 2003, 126, 273-279.
26. K. J. Gallagher, W. Feitknecht and U. Mannweiler, *Nature*, 1968, 217, 1118-1121.
27. S. Zhang, W. Wu, X. Xiao, J. Zhou, F. Ren and C. Jiang, *Nanoscale Res Lett*, 2011, 6, 1-9.
28. G. A. B. Confalonieri, P. Szary, D. Mishra, M. J. Benitez, M. Feyen, A. H. Lu, L. Agudo, G. Eggeler, O. Petracic and H. Zabel, *Beilstein J. Nanotechnol.*, 2010, **1**, 101-107.
29. H. Chen, D. C. Colvin, B. Qi, T. Moore, J. He, O. T. Mefford, F. Alexis, J. C. Gore and J. N. Anker, *J. Mater. Chem.*, 2012, **22**, 12802-12809.
30. M.B. McBride, *Environmental Chemistry of Soils*. Oxford University Press, New York, 1994.
31. A. Zach-Maor, R. Semiat and H. Shemer, *J. Colloid Interface Sci.*, 2011, **363**, 608-614.

Table of Contents

Large cavities embedded with iron oxide nanoparticles within mesocellular siliceous foams (MCFs) uptake phosphate ions from water effluent.